Aerodynamics simulation studies on the observation head placed on a board of the unmanned aerial vehicle

Izabela Krzysztofik[1,*], *Slawomir* Blasiak[2]

[1,2] Faculty of Mechatronics and Mechanical Engineering, Kielce University of Technology, al. Tysiaclecia Panstwa Polskiego 7, 25-314 Kielce, Poland

Abstract. An important element of UAV equipment are observation heads. Observation head is multi-sensor optoelectronic system. It includes TV camera and infrared camera, safe for the eye rangefinder and laser pointer and a navigation system GPS. Image stability is provided by electro-mechanical gyro stability system. Optoelectronic head are designed for use in systems of detection, identification and observation of ground and air targets and in daylight and at night. In this paper simulation studies of the air masses flow around the observation head placed on the UAV deck, for different speeds of UAV movement were conducted. The results of numerical research were presented in a graphical form.

1 Introduction

Nowadays, modern equipment of a modern army includes unmanned aerial vehicles (UAV). The significant role is played by their independency during searching and tracking a target on the ground. One of the basic elements of UAV equipment is an observation head. The head is an optoelectronic system which integrates many sensors: an infrared camera, a daylight camera and an eye-safe laser rangefinder. It can be also equipped with a camera for low light performance, a laser pointer or an illuminator and GPS/IMU inner navigation system. The observation head is for automatic searching and tracking targets which have to be destroyed. It often performs its tasks in circumstances of vibration and interferences coming from UAV maneuvering board [1]. At the same time high accuracy and reliability are demanded. In this situation complex studies on the head are crucial. A wide range of research should include: material analysis, dynamics and control analysis, heat exchange, thermo-flexibility and analysis of developing the components and the elements of the described head, similarly to the studies [2-12]. In the paper [2] the general mathematic dynamics model and the algorithm for controlling the head placed on a moveable base are presented. The paper [3] also presents kinematic of mutual movement of UAV and a ground target and the research on dynamics of the controlled observation head placed on UAV during searching and tracking the target. PD controller was developed to control the head. The papers [4,5] present the analysis of head fuzzy logic controlling and controlling the head axis using the dynamics inverse problem. This paper presents simulation studies on air-masses flowing around the observation head placed on a board of UAV for different UAV speeds. A hypothetical set of observation head – UAV was taken under consideration.

2 Main aim

2.1 Modeling data

The object of the research is a volume of airspace inside which the aerial vehicle is located. The observation head is fixed to the vehicle. The paper describes simulation research for four cruise speeds of the aerial vehicle and determining their influence on the air stream behavior flowing around the head. Using the tool for solid modeling the researchers prepared the spatial model of the aerial object with the observation head (Fig. 1).

Fig. 1. The aerial object with the observation head.

Around the object the cuboid of dimensions (HxWxD) 35x40x50 m was generated. This space was so big to prevent the occurrence of uncontrolled turbulence. The whole aerial object-head system was implemented to Ansys CFX application which is presented in Fig. 2.

* Corresponding author: pssik@tu.kielce.pl

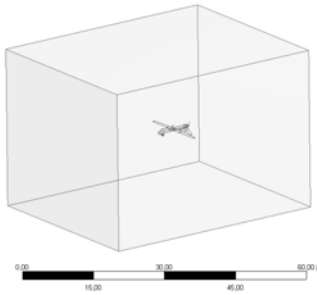

Fig. 2. Isometric view of the aerial object in the volume of air.

2.1 Numerical model

During the calculation process the fluid movement criterion was used to build mathematical model similarly as for pneumatic systems [13,14] in equations describing the physics of flow. In the analysis with using Computational Fluid Dynamics (CFD) the solving systems of transport differential equations are used to obtain detailed information on phenomena taking place in researched physical objects.

Mathematical description of researched phenomena is quite complicated therefore some assumptions and simplification conditions are used:

- Cartesian coordinate system (x, y, z),
- there are no chemical reactions and phase transition,
- gravity forces impact was ignored.

Fluid movement is described by Navier-Stokes equations (2)-(4) which together with the continuity equation (1) are the complete correlation system allowing to determine the pressure and the flow velocity field.

$$\frac{\partial \rho}{\partial t} + div(\rho \mathbf{U}) = 0 \tag{1}$$

Navier-Stokes equations.

$$\frac{\partial(\rho U)}{\partial t} + div(\rho U \mathbf{U}) = -\frac{\partial P}{\partial x} + div(\mu\, grad\, U) + \left[-\frac{\partial\left(\rho \overline{u'^2}\right)}{\partial x} - \frac{\partial\left(\rho \overline{u'v'}\right)}{\partial y} - \frac{\partial\left(\rho \overline{u'w'}\right)}{\partial z} \right] \tag{2}$$

$$\frac{\partial(\rho V)}{\partial t} + div(\rho V \mathbf{U}) = -\frac{\partial P}{\partial y} + div(\mu\, grad\, V) + \left[-\frac{\partial\left(\rho \overline{u'v'}\right)}{\partial x} - \frac{\partial\left(\rho \overline{v'^2}\right)}{\partial y} - \frac{\partial\left(\rho \overline{v'w'}\right)}{\partial z} \right] \tag{3}$$

$$\frac{\partial(\rho W)}{\partial t} + div(\rho W \mathbf{U}) = -\frac{\partial P}{\partial z} + div(\mu\, grad\, W) + \left[-\frac{\partial\left(\rho \overline{u'w'}\right)}{\partial x} - \frac{\partial\left(\rho \overline{v'w'}\right)}{\partial y} - \frac{\partial\left(\rho \overline{w'^2}\right)}{\partial z} \right] \tag{4}$$

where: ρ – fluid density, kg/m^3, μ – dynamic viscosity, kg/ms.

Nowadays, k-ε model is one of the most popular models and it is the most common model of the flow turbulence. Two mathematical units (k-ε) require two additional transport equations which can be described in the form:

$$\frac{\partial(\rho k)}{\partial t} + div(\rho k \mathbf{U}) = div\left(\frac{\mu_t}{\sigma_t} grad\, k\right) + \mu_t \phi - \rho\varepsilon \tag{5}$$

$$\frac{\partial(\rho \varepsilon)}{\partial t} + div(\rho \varepsilon \mathbf{U}) = div\left(\frac{\mu_t}{\sigma_t} grad\, \varepsilon\right) + C_1 \mu_t \frac{\varepsilon}{k}\phi - C_2 \rho \frac{\varepsilon^2}{k} \tag{6}$$

Quantity k means kinetic energy of turbulence and quantity ε means a dissipation of turbulence kinetic energy. The aforementioned partial differential equations are implemented in the calculation module of Ansys CFX application. For final solving of equations set describing turbulent fluid movements it is necessary to provide boundary conditions data which provides a clear solution and decides on a calculation process inside the researched area.

3 Ansys CFX analysis

In Ansys Workbench, Fluid Flow (CFX) -Meching module the non-structural computational grid was generated having 74523 junctions and 360140 elements. The computational grid structure is presented in Fig. 3.

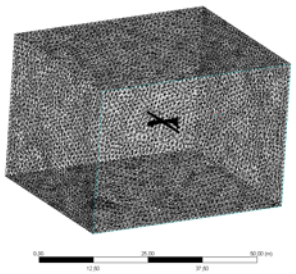

Fig. 3. MES model of the computational grid.

Due to the huge disproportion between the researched area and the aerial vehicle model the density of meshes was increased on the object surface as well as close to the object to – as accurately as possible – reflect its shapes.

Another preliminary stage to the numerical calculations was to determine boundary conditions.

1. At the entry point – Dirichlet criterion – there is the assumption that the air stream velocity (Fig. 4) is equal respectively for the four researched cases: a) 36.14 m/s, b) 40.31 m/s, c) 43.09 m/s and d) 45.87 m/s.
2. At the exit point Neuman Average Static Pressure criterion of 0.1 MPa was assumed.
3. For other surfaces on the cuboid circumference Free Slip Wall boundary conditions were used.

The values of physical quantities were also used for the calculations: ambient temperature T=25^{o}C, density ρ=1.185 kg/m^3, reference pressure p=101325 Pa.

The aerial object cruise speed is much lower than the speed of sound and is within the limits of 130-165 km/h and therefore the air flow was assumed in the low turbulence level – k-ε model.

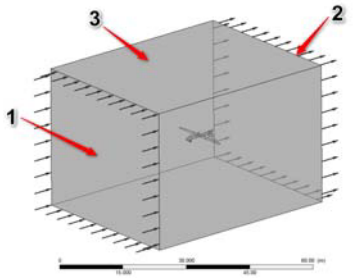

Fig. 4. Boundary conditions assumed to the numerical calculations.

4 Results and discussion

Because of conducting the numerical calculations considering boundary conditions the fields of velocity distribution in cross-section in its plane of the aerial object were determined as first.

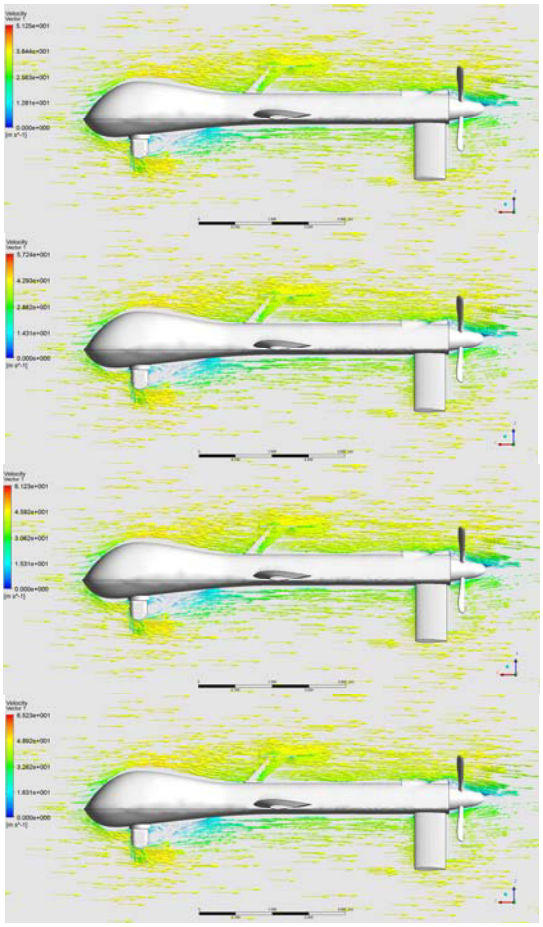

Fig. 5. Velocity vectors distribution in UAV cross-section.

The velocity vectors distribution in UAV cross-section is practically the same for all researched cruise speeds presented in Fig. 5. Only the maximal velocity of the air stream flow – from 51.25 to 65.23 m/s – is changed. The maximal air-masses turbulence can be observed behind the observation head and that may impact on the aerodynamic lift volume which have influence on the whole aerial object and resistances. In front of the head air movements are almost without turbulence.

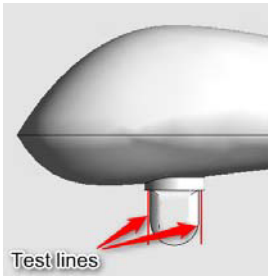

Fig. 6. Test lines for measuring the fluid velocity.

In Fig. 7 there are changes of the fluid velocity along the test lines for the chosen UAV cruise speeds.

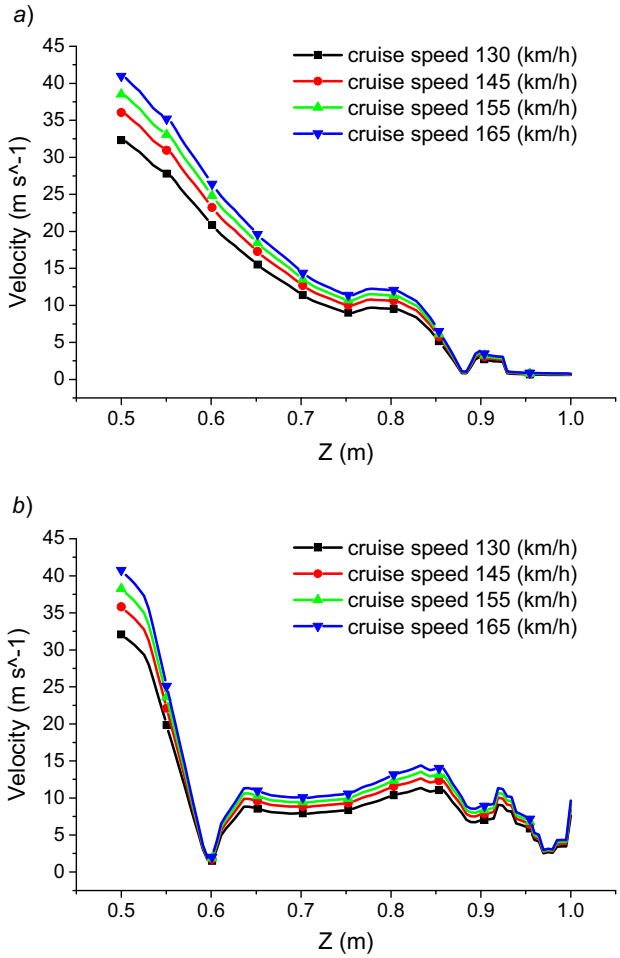

Fig. 7. Velocity in the test lines.

Maximal air-masses velocities in the front test line can be observed in the bottom part of the head. Depending on UAV cruise speed the values are from 32.5 to about 42.5 m/s. At distance of 0.8 m small flow velocity increasing can be observed. It is caused by the gap between the body and the rotating component of the observation head. Another situation of velocity distribution can be observed in the test line just behind the observation head. The velocity close to zero was experienced at distance of 0.6 m and at distance of 0.6-1.0 m the velocity did not exceed 15 m/s. The sharpest velocity change can be observed at distance of 0.5-0.6 m. In Fig. 8 there are the fields of pressure distribution impacting on the body of the aerial object and the head fixed on it for speeds of 36.14 m/s and 45.87 m/s.

Maximal pressure values (fields marked with red) can be observed in the vehicle part in front of the body forefront and in the part anterior to the observation head. For the chosen cruise speeds the maximal pressure values are almost the same (see Fig. 9).

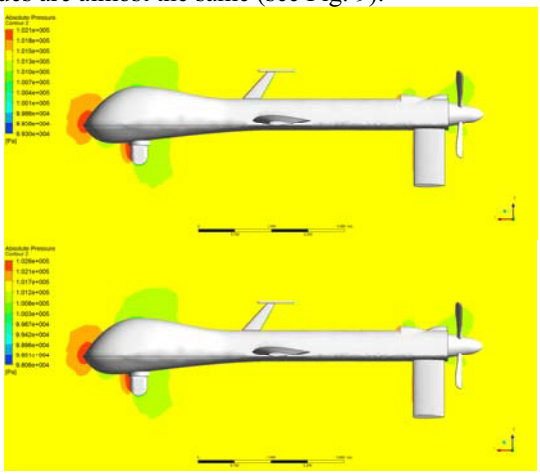

Fig. 8. Fields of pressure distribution impacting on the aerial object body and the head.

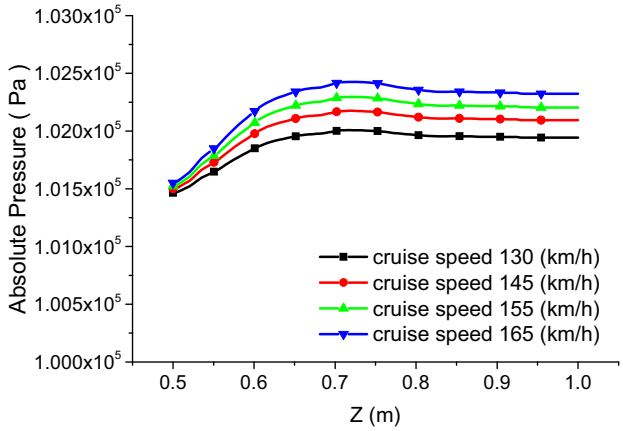

Fig. 9. Pressure in the front test line.

During the simulation studies it was assumed that the aerial object moved with low cruise speeds from 130 to 165 km/h. Choosing the range of cruise speeds was not without impact on Mach number distribution in the assessed area. In Fig. 10 it can be noticed that the maximal local Mach number for the speed of 130 km/h is 0.148 and for the speed of 165 km/h is 0.1884.

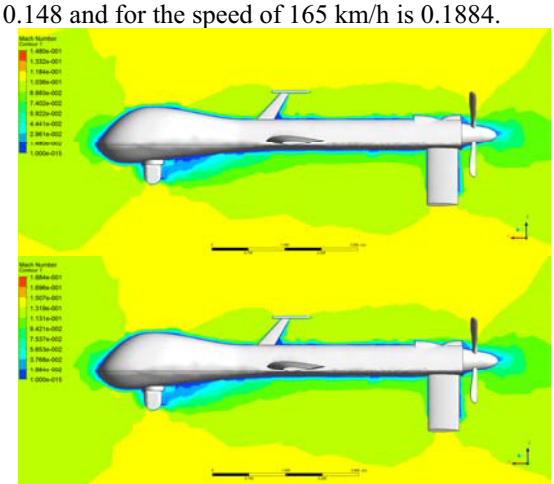

Fig. 10. Mach number distribution in UAV cross-section.

5 Conclusions

For the unmanned aerial vehicles the resistance values of the air-masses flowing around them are very important. As it is known, by minimising aerodynamic resistance the cruise range can be increased. Not without significance for the ground personnel controlling the object is the fact of possibility of speed increasing and making instantaneous acceleration. The prepared numerical model of air flowing around the whole aerial object and the observation head fixed to it which bases on CFD can be useful for shape designing and all UAV elements optimising. Using the presented model you can develop aerodynamic characteristics by changing their structures. In the further studies the shape and the construction of the observation head can be also considered. The prepared algorithm is a very useful calculation tool helping the designers of these types of devices. The obtained results should be experimentally verified in a wind tunnel.

References

1. Z. Koruba, Ladyzynska-Kozdras E., J. Theor. Appl. Mech. **48**(3), 551-566 (2010)
2. I. Krzysztofik, Z. Koruba, J. Autom. Inf. Sci. **44**(5), 38-47 (2012)
3. I. Krzysztofik, Z. Koruba, J. App. Math. **2014**, Article ID 934250 (2014)
4. I. Krzysztofik, *Proceedings of 22nd International Conference on Engineering Mechanics 2016*, 326-329 (Academy of Sciences of the Czech Republic, 2016)
5. D. Gapinski, I. Krzysztofik, *Proceedings of the 15th International Carpathian Control Conference* (ICCC), 129-134 (2014)
6. J. E. Takosoglu, *Proceedings of 22nd International Conference on Engineering Mechanics 2016*, 546-549 (Academy of Sciences of the Czech Republic, 2016)
7. S. Blasiak J. Therm. Sci. Technol. **10**(1), JTST0016 (2015)
8. S. Blasiak, C. Kundera. Procedia Eng. **39**, 315-326 (2012)
9. S. Blasiak, J. E. Takosoglu, P.A. Laski, J. Therm. Sci. Technol. **9**(2), JTST0011 (2014)
10. M. Piasecka, Int. J. Heat Mass Transf. **81**, 114-121 (2015)
11. L. Nowakowski, M. Wijas, *Proceedings of 22nd International Conference on Engineering Mechanics 2016*, 430-433 (Academy of Sciences of the Czech Republic, 2016)
12. L. Nowakowski, E. Miko, M. Skrzyniarz, *Proceedings of 22nd International Conference on Engineering Mechanics 2016*, 426-429 (Academy of Sciences of the Czech Republic, 2016)
13. P. A. Laski, J. E. Takosoglu, S. Blasiak. Robot. Auton. Sys. **72**, 59-70 (2015)
14. J. E. Takosoglu, P. A. Laski, S. Blasiak, G. Bracha, D. Pietrala, Meas. Cont. **49**(2), 62-71 (2016)

This research was supported in part by PLGrid Infrastructure.